Research Square

Preprints are preliminary reports that have not undergone peer review.
They should not be considered conclusive, used to inform clinical practice,
or referenced by the media as validated information.

TIPE2 suppresses adipogenesis via METTL14-mediated m6A methylation and represents a potential therapeutic target for obesity

Xinxin Xiang

xingxinxin1592@163.com

Zibo Central Hospital Affiliated to Shandong Medical University

Chuanjie liang

Zibo Central Hospital Affiliated to Shandong Medical University https://orcid.org/0009-0000-8461-8040

Yangjunjie Wang

Zibo Central Hospital Affiliated to Shandong Medical University

Wenxiang Zheng

Zibo Central Hospital

Wenxiu Tian

Zibo Central Hospital Affiliated to Shandong Medical University

Chuanqin Shi

Zibo Central Hospital

Tianchu Li

Zibo Central Hospital Affiliated to Shandong Medical University

Wing-Kin Syn

Saint Louis University

Patricia Aspichueta

University of the Basque Country

Xiaodong Zhao

Zibo Central Hospital Affiliated to Shandong Medical University

Wei Hou

Qilu Medical University

Article

Keywords: TIPE2, m6A, METTL14, PPAR-γ, Adipogenic differentiation, Obesity

Posted Date: November 16th, 2026

DOI: https://doi.org/10.21203/rs.3.rs-11199357/v1

License: This work is licensed under a Creative Commons Attribution 4.0 International License.
Read Full License

Additional Declarations:
(Not answered)

Table 1 and 2 are available in the Supplementary Files section.

TIPE2 suppresses adipogenesis via METTL14-mediated m6A methylation and represents a potential therapeutic target for obesity

Authors

Chuanjie Liang,[1] Yangjunjie Wang,[2] Wenxiang Zheng,[1] Wenxiu Tian,[1] Chuanqin Shi,[1] Tianchu Li,[1] Wing-Kin Syn,[3,4,5] Patricia Aspichueta,[6,7,8] Xiaodong Zhao,[9,*] Wei Hou,[10,*] Xinxin Xiang,[1,11*]

Affiliations

[1]Translational Medicine Center, Zibo Central Hospital Affiliated to Shandong Medical University, Zibo 255000, Shandong, China.

[2]Department of Nuclear Medicine and Radiotherapy, Zibo Central Hospital Affiliated to Shandong Medical University, Zibo 255000, Shandong, China.

[3]Department of Internal Medicine, Division of Gastroenterology and Hepatology, Saint Louis University School of Medicine, St. Louis, MO, USA.

[4]Department of Physiology, Faculty of Medicine and Nursing, University of Basque Country UPV/EHU, Vizcaya, Spain.

[5]Department of Pathology, Saint Louis University, St Louis, MO, USA.

[6]Centro de Investigación Biomédica en Red de Enfermedades Hepáticas y Digestivas (CIBEREHD), Instituto de Salud Carlos III, Madrid, Spain.

[7]Department of Physiology, Faculty of Medicine and Nursing, University of the Basque Country (UPV/EHU), Leioa, Spain.

[8]Biobizkaia Health Research Institute, Barakaldo, Spain.

[9]Department of Endocrinology, Zibo Central Hospital Affiliated to Shandong Medical University, Zibo 255000, Shandong, China.

[10]Translational Medicine Research Center, School of Clinical Medicine, Qilu Medical University, Zibo 255300, China.

[11]College of Life Sciences, Ludong University, Yantai 264000, Shandong, China.

* Corresponding authors.

E-mail addresses: 19xiaodong@163.com(X.D.Z.), houwei@qlmu.edu.cn(W.H.), xiangxinxin1592@163.com (X.X.X.).

ABSTRACT

Despite conserved mechanisms maintaining energy homeostasis, the global obesity epidemic continues to rise. Tumor necrosis factor-α-induced protein 8-like 2 (TIPE2) is an anti-inflammatory regulator essential for immune homeostasis, yet its role in adipogenesis remains unclear. Here, we show that TIPE2 expression in human adipose tissue is inversely correlated with body mass index (BMI) and metabolic dysfunction. In mice, Tipe2 deficiency exacerbates diet-induced obesity, hyperglycaemia, and insulin resistance, whereas systemic AAV-mediated TIPE2 overexpression alleviates these phenotypes. In vitro, TIPE2 suppresses adipogenic differentiation in primary preadipocytes. Mechanistically, TIPE2 regulates N6-methyladenosine (m6A) via m6A methyltransferase-like 14 (METTL14). Loss of TIPE2 reduces m6A levels and METTL14 expression, whereas METTL14 restoration reverses the pro-adipogenic effects. Furthermore, TIPE2 modulates adipogenesis through peroxisome proliferator-activated receptor-γ (PPAR-γ) signaling. Together, these findings identify TIPE2 as a suppressor of adipogenesis via coordinated regulation of METTL14-dependent m6A modification and PPAR-γ signaling.

Keywords TIPE2; m6A; METTL14; PPAR-γ; Adipogenic differentiation; Obesity.

INTRODUCTION

Currently, the prevalence of obesity is increasing, seriously affecting people's quality of life and health[1]. Obesity is caused by an imbalance between energy intake and expenditure, characterized by excessive lipid accumulation in adipose tissue leading to low-grade chronic inflammation and metabolic disorders[2,3].

The regulation of adipogenesis involves complex transcriptional and epigenetic cascades. PPAR-γ is a member of the nuclear receptor superfamily and is necessary and sufficient for adipogenic differentiation. PPAR-γ and CCAAT/enhancer-binding protein-α (C/EBP-α) activate target genes for terminal adipogenic differentiation along with other transcription factors[4]. In recent years, the role of epigenetic regulation in lipid metabolism disorders has attracted widespread attention. Epigenetic modifications mainly include DNA methylation, RNA modification, and protein modification[5]. RNA modification is an important branch of epigenetics. More than 150 different types of chemical modifications have been found, with m6A being the most abundant RNA modification.

Recent studies have shown that m6A modification is closely related to obesity and plays an important regulatory role in biological processes including adipogenesis, lipid metabolism, and insulin resistance[6,7]. m6A modification is a crucial post-transcriptional modification involving the addition of a methyl group at the N6 position of adenosine[8]. The dynamic reversible control of m6A modification is carried out by methyltransferases and demethylases. m6A-binding proteins recognize m6A methylation, reducing the stability of target transcripts thereby influencing biological functions[9]. Emerging evidence indicates that it has been demonstrated that m6A-related enzymes play important roles in lipid metabolism. Studies have found that m6A demethylase fat mass and obesity associated (FTO) is closely related to lipogenesis and lipolysis, in which the level of m6A is negatively correlated with the expression of FTO, and FTO knockdown inhibits 3T3-L1 preadipocytes differentiation[10,11]. m6A methyltransferases methyltransferase-like 3 (METTL3), METTL14, and Wilms tumor 1-associated protein (WTAP) have been shown to influence lipid production in mouse preadipocytes by regulating mitotic clone expansion[12]. However, there is limited research on the role of methyltransferase METTL14 in adipogenesis which requires further elucidation.

TIPE2 is the third member of the TNFAIP8 family. It has been well documented as a key inhibitor of inflammation and autoimmunity, with protective roles in disorders such as atherosclerosis, systemic lupus erythematosus (SLE), and rheumatoid arthritis[13,14]. In atherosclerosis, TIPE2 attenuates disease progression by modulating vascular smooth muscle cell responses to oxidized low-density lipoprotein[15,16]. TIPE2 expression is reduced in collagen-induced arthritis and negatively correlates with disease severity. Moreover, ectopic TIPE2 expression suppresses the development of rheumatoid arthritis, in part through inhibition of signal transducer and activator of transcription and nuclear factor kappa-B signaling pathways (NF-κB) within joint tissues[17]. In a mouse model of SLE, TIPE2 overexpression markedly ameliorates disease manifestations by driving macrophage polarization towards an anti-inflammatory M2 phenotype[18]. Despite these advances, the contribution of TIPE2 to metabolic regulation remains largely unexplored.

This study aimed to investigate the expression pattern and relevant signaling pathways of TIPE2 during adipogenesis. Elucidating how TIPE2 regulates the differentiation of adipocytes, may provide new insights to potential therapies for obesity and other metabolic diseases.

Materials and methods

Human subjects

Subcutaneous adipose tissue samples were obtained from 35 patients undergoing abdominal surgery for non-malignant conditions at Zibo Central Hospital. Peripheral blood samples were collected intraoperatively. Immediately after surgical excision, adipose tissues were snap-frozen in liquid nitrogen and stored at −80 °C until analysis. Detailed clinical and demographic characteristics of the enrolled participants are summarized in table 1. The study protocol was approved by the Institutional Ethics Committee of Zibo Central Hospital, and written informed consent was obtained from all participants in accordance with the principles of the Declaration of Helsinki.

Experimental animals

Eight-week-old ob/ob mice and wild-type (WT) mice were purchased from Beijing Pengyue Company. Male WT and Tipe2$^{-/-}$ mice on a C57BL/6 background (8-10 weeks old) were also obtained from the same supplier. Mice were housed under specific pathogen-free (SPF) conditions at 24°C with 55% humidity under a 12 h light/dark cycle and had ad libitum access to food and water. Animals were acclimated for 1 week prior to experimentation.

All animal experiments were approved by the Institutional Animal Care and Use Committee of Zibo Central Hospital.

Diet-induced obesity (DIO) mouse model

Male C57BL/6 mice were randomly assigned to either a normal chow diet (NCD) group or a high-fat diet (HFD) group and maintained on the respective diets for 12 consecutive weeks. The HFD consisted of 60% kcal from fat, 20% kcal from carbohydrates, and 20% kcal from protein, whereas the NCD contained 10% kcal from fat, 70% kcal from carbohydrates, and 20% kcal from protein.

Isolation of primary preadipocytes from epididymal adipose tissue

Primary preadipocytes were isolated from epididymal adipose tissue using a collagenase digestion protocol. Briefly, mice were euthanized by cervical dislocation and sterilized in 75% ethanol for 15 min prior to tissue collection under sterile conditions. Epididymal fat pads were

excised, rinsed with phosphate-buffered saline (PBS), and minced into small fragments. Tissues were digested in collagenase solution at 37°C with gentle shaking (120 rpm) for 40 min until a homogeneous suspension formed. Following digestion, samples were diluted with phenol red-free DMEM and filtered through a 200-mesh cell strainer. The stromal vascular fraction was collected, washed twice with PBS, and centrifuged sequentially at 500 rpm for 5 min and 2,400 rpm for 10 min. Cell pellets were resuspended in complete culture medium and seeded into six-well plates. After 24 h, the medium was replaced to remove debris and non-adherent cells.

Cell culture and adipogenic differentiation

Mouse 3T3-L1 preadipocytes were cultured in high-glucose DMEM supplemented with 10% fetal bovine serum (FBS). Cells were seeded into six-well plates and grown to full confluence. Two days after reaching confluence (designated day 0), adipogenic differentiation was induced using differentiation medium containing high-glucose DMEM supplemented with 10% FBS, 10 μg/mL insulin (Sigma-Aldrich), 1 μM dexamethasone (DEX; Sigma-Aldrich), and 0.5 mM 3-isobutyl-1-methylxanthine (IBMX; Sigma-Aldrich). After 72 h, cells were switched to maintenance medium containing 10% FBS and 10 μg/mL insulin for an additional 6 days, followed by culture in growth medium. Differentiation efficiency was assessed by Oil Red O staining on day 12.

Lentivirus Production

The viral vectors were transfected into HEK293T cells using Lipofectamine 2000 (Invitrogen; Thermo Fisher Scientific, Inc.) together with the packaging plasmids psPAX2 and pMD2.G Infectious lentiviruses were harvested at 72 h post-transfection, and cell debris was removed by rapid centrifugation followed by filtration through 0.45 μm cellulose acetate filters. Viral titers were determined by fluorescence-activated cell sorting (FACS) analysis of GFP-positive HEK293T cells and were approximately 1×10^9 transducing units (TU)/mL. The lentiviral stocks were stored at −80°C for further use.

AAV9 Virus Production and Injection

AAV9 virus was produced by GeneChem. The full-length coding sequence of mouse TIPE2 (GenBank: NM_027206.3) was cloned into the GV825 vector containing the CMV-MCS-3Flag-FT2A-EGFP-WPRE-BGH polyA cassette through Nhe and AgeI restriction sites using an In-

Fusion recombination strategy. Recombinant vectors were verified by DNA sequencing and subsequently packaged into AAV9. The packaged virus was designated as AAV9-CMV-TIPE2, and the corresponding empty vector virus was used as the negative control. The viral titer was 5.00×10^{12} v.g./mL, as determined by quantitative PCR. For *in vivo* administration, AAV9-CMV-Tnfaip8l2 virus was delivered via tail vein injection at a dose of 20 μL per injection site, with 3–5 injection sites per mouse. AAV9 Virus Production and Injection.

OGTT and ITT

For OGTT assays, mice were fasted overnight for 12 h and administered glucose (2 g/kg body weight) by oral gavage. Blood glucose concentrations were measured from tail vein blood at 0, 15, 30, 60, 90, and 120 min using a glucometer. For ITT assays, mice were allowed to recover for 1 week following OGTT. After a 6 h fast, insulin (1 U/kg body weight) was administered intraperitoneally, and blood glucose levels were monitored at the indicated time points. The AUC was calculated to quantify glucose and insulin tolerance.

Immunohistochemistry

Adipose tissue samples were fixed in adipose tissue fixative solution (Servicebio), embedded in paraffin, and sectioned at 4 μm thickness. Following deparaffinization and antigen retrieval in citrate buffer (pH 6.0), sections were blocked with 5% bovine serum albumin (BSA; Solarbio) and incubated with primary antibodies overnight at 4°C. Sections were subsequently incubated with horseradish peroxidase (HRP)-conjugated secondary antibodies (Servicebio), developed using a DAB substrate kit (Servicebio), and counterstained with hematoxylin.

Measurement of Serum TG and TC Levels

Serum TG and TC concentrations were measured using commercial assay kits (Nanjing Jiancheng Bioengineering Institute) according to the manufacturer's instructions. Briefly, 2.5 μL serum or standard solution was mixed with 250 μL working reagent in 96-well plates and incubated at 37°C for 10 min. Absorbance values were measured, and concentrations were calculated from standard curves and expressed as mmol/L.

Oil Red O staining

Differentiated adipocytes were washed three times with PBS and fixed with 4% paraformaldehyde for 10 min. Cells were incubated with 60% isopropanol for 30 min and stained with Oil Red O solution (Sigma-Aldrich) for 30 min at room temperature. Excess dye

was removed with 60% isopropanol followed by PBS washes. Lipid accumulation was visualized using an inverted microscope.

Fluorescent staining of lipid droplets

Differentiated adipocytes were seeded into culture dishes and incubated overnight at 37°C in a humidified incubator containing 5% CO_2. Cells were washed twice with PBS and incubated with Lipi-series fluorescent dye working solution (Dojindo Laboratories) at 37°C for 30 min. Fluorescence images were captured using an epifluorescence microscope.

RNA extraction and real-time RT-qPCR

Total RNA was isolated using TRIzol reagent (Invitrogen) according to the manufacturer's instructions. Complementary DNA (cDNA) was synthesized from 2 μg total RNA using the PrimeScript RT reagent kit (Takara). Quantitative PCR was performed using SYBR Green Master Mix (Vazyme) on a 7500 Real-Time PCR System (Thermo Fisher Scientific). Relative gene expression was normalized to housekeeping genes using the 2^-ΔΔCt method. Primer sequences are listed in table 2.

Western blotting

Samples were lysed in RIPA buffer supplemented with protease inhibitors. Lysates were centrifuged at 4°C for 10 min, and protein concentrations were determined using a BCA assay. Equal amounts of protein (80 μg) were separated by SDS-PAGE and transferred onto nitrocellulose membranes. Membranes were blocked with 5% non-fat milk for 1 h at room temperature and incubated with primary antibodies overnight at 4°C. After washing, membranes were incubated with HRP-conjugated secondary antibodies (1:10,000; Boster Biological Technology) and visualized using enhanced chemiluminescence reagents. Detailed antibody information is provided in the table 2.

Co-immunoprecipitation assay

Cells were lysed in IP lysis buffer containing protease inhibitor cocktails. Lysates were incubated with the indicated primary antibodies overnight at 4°C followed by incubation with Protein A/G agarose beads. Immunoprecipitated proteins were washed extensively, resolved by SDS-PAGE, and transferred to nitrocellulose membranes. Membranes were blocked with 5% non-fat milk and incubated with the indicated antibodies. Protein bands were visualized using chemiluminescent substrate.

Dot blot assay for global m6A detection

Total RNA samples were denatured at 65°C for 5 min and spotted onto nitrocellulose membranes. Following UV crosslinking, membranes were washed with PBST, blocked with 5% non-fat milk, and incubated with anti-m6A antibody overnight at 4°C. Membranes were then incubated with secondary antibodies for 1 h at room temperature and visualized using a chemiluminescence imaging system.

Quantification of global m6A RNA methylation

Global m6A levels were quantified using the EpiQuik m6A RNA Methylation Quantification Kit (Epigentek) according to the manufacturer's protocol. Briefly, total RNA samples were added to assay wells and incubated at 37°C for 90 min. Capture antibodies, detection antibodies, and enhancer solutions were sequentially added. Colorimetric signals were developed and measured spectrophotometrically. Relative m^6^A levels were calculated using a standard curve.

MeRIP-qPCR

Total RNA was extracted and purified to remove ribosomal RNA contamination. RNA was fragmented into ~100 nt fragments and denatured prior to immunoprecipitation. Fragmented RNA was incubated overnight at 4°C with anti-m6A antibody and Protein A/G magnetic beads in immunoprecipitation buffer supplemented with RNase inhibitors. Immunoprecipitated methylated RNA was eluted and purified for downstream RT-qPCR analysis.

Flow cytometry staining

Cells were stained with fluorophore-conjugated antibodies against CD45, CD31, and Ter119 to exclude hematopoietic, endothelial, and erythroid cell populations. Neutral lipid dyes (BODIPY) were used to identify lipid-containing adipocytes. For intracellular PLIN1 staining, cells were fixed and permeabilized prior to antibody incubation. Viability dyes, fluorescence-minus-one (FMO) controls, and single-color compensation controls were included to ensure accurate gating and compensation. Flow cytometric data were acquired and analyzed using FlowJo software.

Statistical analysis

Statistical analyses were performed using GraphPad Prism software. Data distribution was assessed for normality prior to statistical analysis. Statistical significance was determined using

two-tailed Student's t-tests, one-way ANOVA, or two-way ANOVA as appropriate. For nonparametric multiple-group comparisons, Kruskal–Wallis tests were performed. Data are presented as mean ± SEM. p value < 0.05 was considered statistically significant

Ethics statement

Human subcutaneous adipose tissue samples were obtained from patients undergoing elective liposuction surgery at Zibo Central Hospital. The collected adipose tissue represented surgical waste and was used exclusively for scientific research. The requirement for written informed consent was waived by the Ethics Committee of Zibo Central Hospital Affiliated to Shandong Medical University because sample collection involved no additional intervention and did not affect patient privacy. The study was approved by the Ethics Committee of Zibo Central Hospital Affiliated to Shandong Medical University (Approval No. 20250261).

All animal experiments were performed in accordance with the National Institutes of Health Guide for the Care and Use of Laboratory Animals and were approved by the Animal Ethics Committee of Shandong Medical University (Approval No. 20240104).

RESULTS

TIPE2 expression is negatively associated with BMI and obesity-related metabolic disorders

To investigate the association between TIPE2 and obesity, we first analyzed the public human adipose tissue transcriptome dataset GSE273902. Differential expression analysis revealed a significant upregulation of TIPE2 in adipose tissue from the Weight-loss group (WL) compared with obese subjects (Obesity), as illustrated by the volcano plot (Figure 1A). Hierarchical clustering analysis showed that TIPE2 clustered among genes enriched in the Weight-loss group but reduced in obese subjects, indicating that TIPE2 expression is suppressed in obesity and restored after weight loss (Figure 1B). Correlation analysis further revealed that TIPE2 expression was positively associated with several metabolic genes and negatively correlated with inflammatory markers, positioning it as a potential regulator of metabolic homeostasis during weight loss (Fig 1C).

To further illustrate the magnitude of TIPE2 reduction within the same cohort, we extracted and compared TIPE2 expression levels between lean and obese subjects from the GSE273902 dataset. Consistently, TIPE2 expression was markedly lower in obese individuals than in WL group (Figure 1D), confirming that TIPE2 is robustly suppressed in obesity.

We next examined TIPE2 expression in subcutaneous adipose tissue from 35 individuals

undergoing abdominal surgery. Participants were stratified into non-obese (Control) (BMI<28 kg/m², n=27) and obese (BMI⩾28kg/m², n=8) groups (table 1). TIPE2 expression showed a significant inverse correlation with BMI, indicating that increased BMI was associated with decreased TIPE2 levels (Figure 1E). TIPE2 expression progressively decreased with increasing BMI and showed a strong negative correlation with BMI ($r = -0.616$, $p<0.0001$; Figure 1F).

At the protein level, western blot analysis further confirmed that TIPE2 protein abundance is reduced under obese conditions (Figure 1F). Moreover, serum triglyceride (TG) levels were inversely correlated with TIPE2 expression ($r=-0.693$, $p<0.001$; Figure 1G).

Immunohistochemical staining of subcutaneous adipose tissue revealed robust TIPE2 expression in adipocytes from lean controls, whereas obese samples exhibited markedly weaker staining, indicating a substantial loss of TIPE2 at the tissue level (Figure 1H). Quantification confirmed a significant reduction of TIPE2-positive area in obese adipose tissue.

Collectively, these results demonstrate that TIPE2 is consistently downregulated in obesity at both the transcript and protein levels and is negatively associated with BMI and TG levels, implicating TIPE2 in obesity-related metabolic dysregulation.

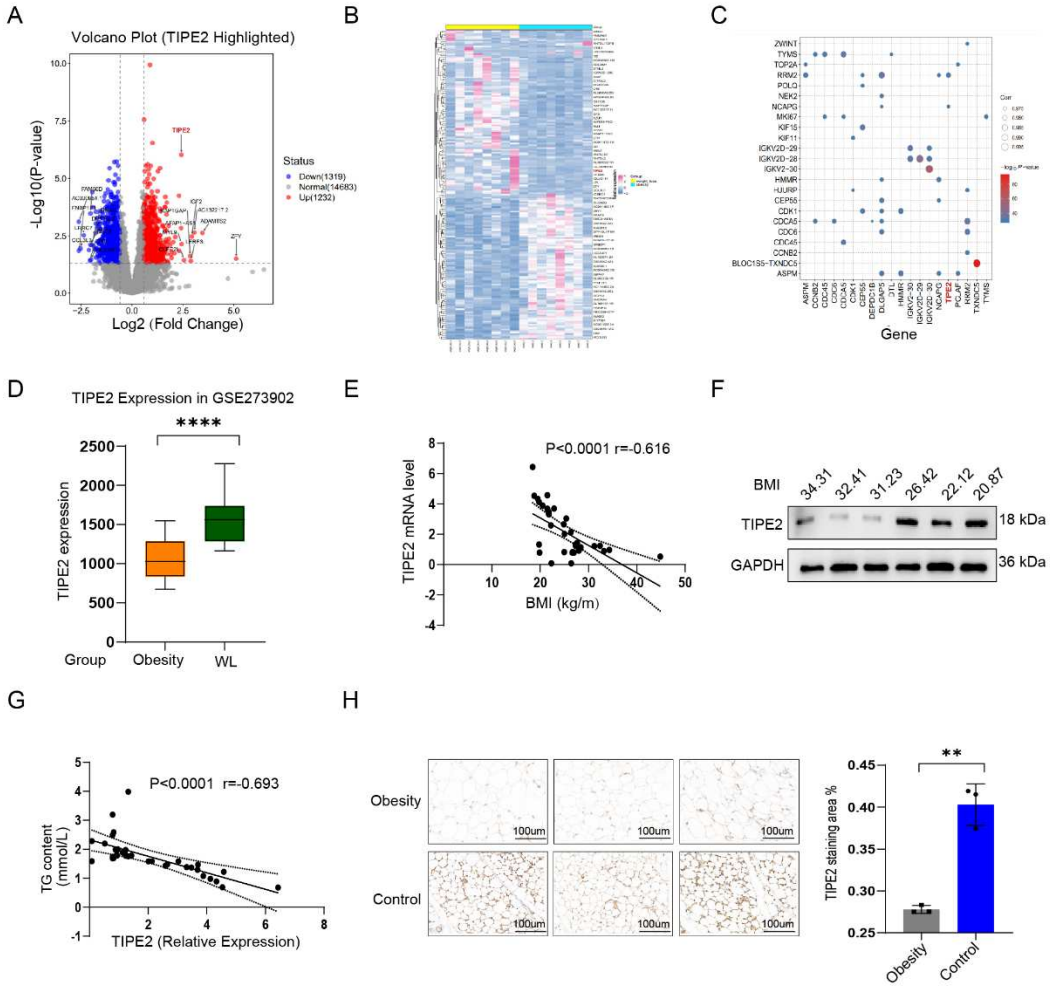


Fig 1 Downregulation of TIPE2 in obese individuals and its correlation with BMI.

(A)Volcano plot of differentially expressed genes (DEGs) between obese and control groups (GSE273902 dataset).

(B)Heatmap of differentially expressed genes in obesity.

(C)Correlation analysis between TIPE2 expression and metabolic genes.

(D)Relative TIPE2 expression in lean and obese individuals from the same GSE273902 cohort.

(E)Correlation analysis of TIPE2 mRNA expression with BMI (n =35).

(F)Western blot analysis of TIPE2 protein levels in adipose tissues from individuals with different BMI values.

(G)Correlation analysis of TG levels and TIPE2 expression (n =35).

(H) Immunohistochemistry of TIPE2 expression in adipose tissue from obese and control individuals (scale bar= 100 μm).

Data are presented as mean ± SEM from at least three independent experiments. **P < 0.01.

TIPE2 protects against diet-induced obesity and improves glucose tolerance and insulin sensitivity in mice.

To determine the role of TIPE2 in obesity and metabolic regulation, we first examined TIPE2 protein expression in adipose tissue. As shown in Figures 2A and 2B, TIPE2 expression was markedly reduced

in *ob/ob* mice compared with wild-type (WT) mice. Consistently, high-fat diet (HFD) feeding significantly decreased TIPE2 protein levels in adipose tissue of C57BL/6 mice relative to those fed a normal chow diet (NCD) (Figures 2C and 2D). To further investigate the metabolic function of TIPE2 *in vivo*, we generated whole-body *Tipe2* knockout (*Tipe2*$^{-/-}$) mice (Figure 2E). Under both NCD and HFD conditions, TIPE2 deficiency led to significantly greater body weight gain compared with WT mice (Figure 2F). Consistently, visceral adipose tissue (VAT) mass and brown adipose tissue (BAT) mass were markedly increased in TIPE2-deficient mice (Figure 2G and 2H). *Tipe2*$^{-/-}$ mice showed significantly elevated plasma total cholesterol (TC) and TG levels (Figure 2I). Metabolic testing demonstrated impaired glucose tolerance in mice, as evidenced by elevated blood glucose levels and an increased area under the curve (AUC) during oral glucose tolerance testing (OGTT) (Figure 2J). Similarly, insulin tolerance testing (ITT) showed decreased insulin sensitivity in *Tipe2*$^{-/-}$ mice (Figure 2K), accompanied by higher homeostasis model assessment of insulin resistance (HOMA-IR) scores and increased serum resistin concentrations (Figure 2L and 2M).

Collectively, these findings demonstrate that TIPE2 protects mice against diet-induced obesity and metabolic dysfunction, and improves glucose tolerance and insulin sensitivity.

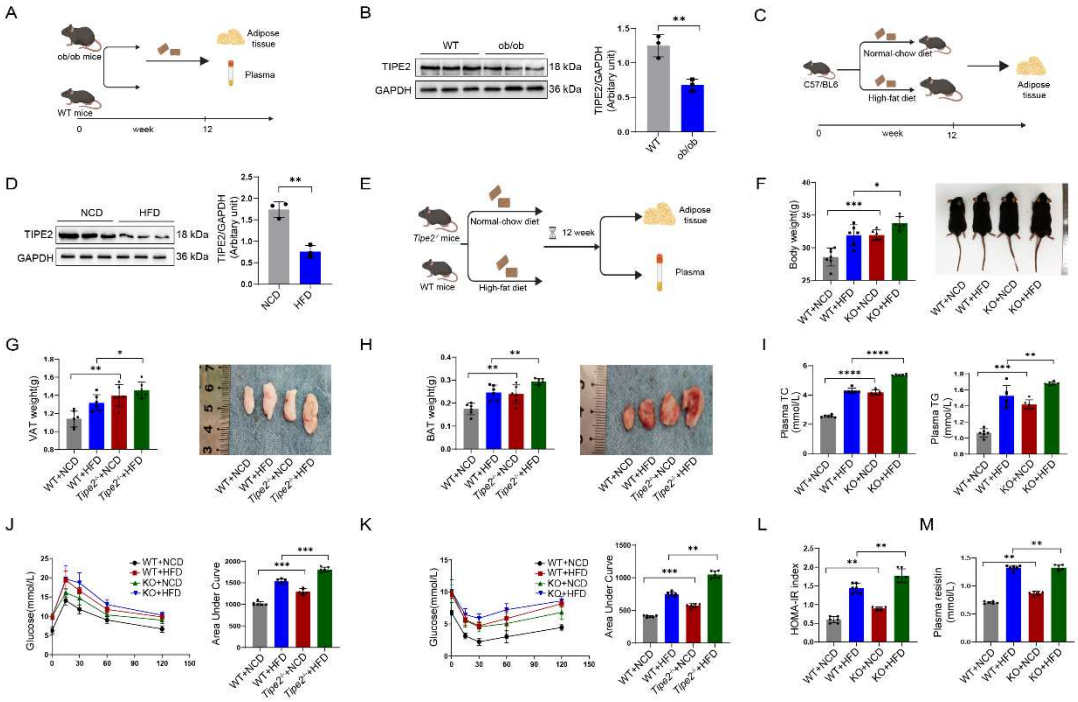


Fig 2 *Tipe2*$^{-/-}$ mice showed significant high-fat diet-induced obesity and impaired glucose tolerance.

(A)*Schematic of the experimental design: ob/ob and WT mice were monitored for 12 weeks, and adipose tissue and plasma were collected at the endpoint for analysis.*

(B)TIPE2 protein levels in EAT of *ob/ob* mice and *WT* mice (n=3).

(C)Expression levels of TIPE2 in different energy states.

(D)C57/BL6 mice were fed with either a normal-chow diet or a high-fat diet for 12 weeks to establish the diet-induced obesity model (n=3).

(E)*Tipe2*$^{-/-}$ and WT mice were maintained on NCD or HFD. After 12 weeks, mice were sacrificed to harvest adipose tissues and blood plasma for further analysis.

(F)Body weight and representative images of mouse from *Tipe2*$^{-/-}$group and WT mice fed with NCD or HFD (n=6).

(G)VAT weight and representative images of adipose tissue (n=6).

(H)BAT weight and representative images of adipose tissue (n=6).

(I)TG and TC levels of *Tipe2*$^{-/-}$group and WT mice fed with NCD and HCD (n=6).

(J)OGTT experimental blood glucose curve and AUC of *Tipe2*$^{-/-}$group and WT mice (n=6).

(K)ITT experimental blood glucose curve and AUC of *Tipe2*$^{-/-}$group and WT mice (n=6).

(L)The level of HOMA-IR of *Tipe2*$^{-/-}$group and WT mice (n=6).

(M)Serum levels of total resistin of *Tipe2*$^{-/-}$group and WT mice (n=6).

Data are presented as mean ± SEM. *P < 0.05, **P < 0.01, ***P < 0.001, ****P < 0.0001.

TIPE2 is upregulated during adipogenic differentiation.

To investigate the role of TIPE2 in adipogenesis, we first measured its expression during 3T3-L1 preadipocytes differentiation. Oil Red O staining revealed a gradual increase in lipid accumulation as differentiation progressed (Figure S1A), and lipid droplet staining showed a concomitant increase in fluorescence intensity upon differentiation (Figure 3A). Reverse transcription quantitative PCR (RT-qPCR) analysis confirmed that TIPE2 mRNA levels were markedly elevated during adipogenesis, along with increased expression of adipogenic markers PPAR-γ and C/EBP-α (Figures 3B and 3C). Western blot analysis further validated that TIPE2 protein levels were upregulated during 3T3-L1 preadipocytes differentiation (Figure 3D). To validate these findings in human preadipocytes cells, we performed a similar analysis. Lipid droplet staining and Oil Red O staining demonstrated increased lipid accumulation and fluorescence intensity in differentiated cells compared with undifferentiated controls (Figure 3E and S1B). Consistent with the 3T3-L1 cells finding, TIPE2 mRNA expression was significantly elevated during the differentiation of human preadipocytes, in parallel with PPAR-γ and C/EBP-α induction (Figures 3F and 3G). Western blot results confirmed that TIPE2 protein expression increased along with adipogenic markers (Figure 3H). We next assessed TIPE2 expression in mouse primary preadipocytes. Flow cytometry analysis verified high purity of the preadipocyte population (Figure S2). As expected, lipid droplet staining and Oil Red O staining revealed increased lipid accumulation and fluorescence intensity in differentiated adipocytes (Figure 3I and S1C). RT-qPCR

results showed that TIPE2 expression was significantly upregulated during adipogenic differentiation, with a similar trend for PPAR-γ and C/EBP-α (Figures 3J and 3K). Western blotting confirmed higher protein levels of TIPE2, PPAR-γ and C/EBP-α in differentiated mouse adipocytes compared with undifferentiated controls (Figure 3L). Together, these findings demonstrate that TIPE2 expression is induced during adipogenic differentiation in 3T3-L1 preadipocytes, human preadipocyte and mouse primary preadipocytes, suggesting that TIPE2 may play a conserved role in the regulation of adipogenesis.

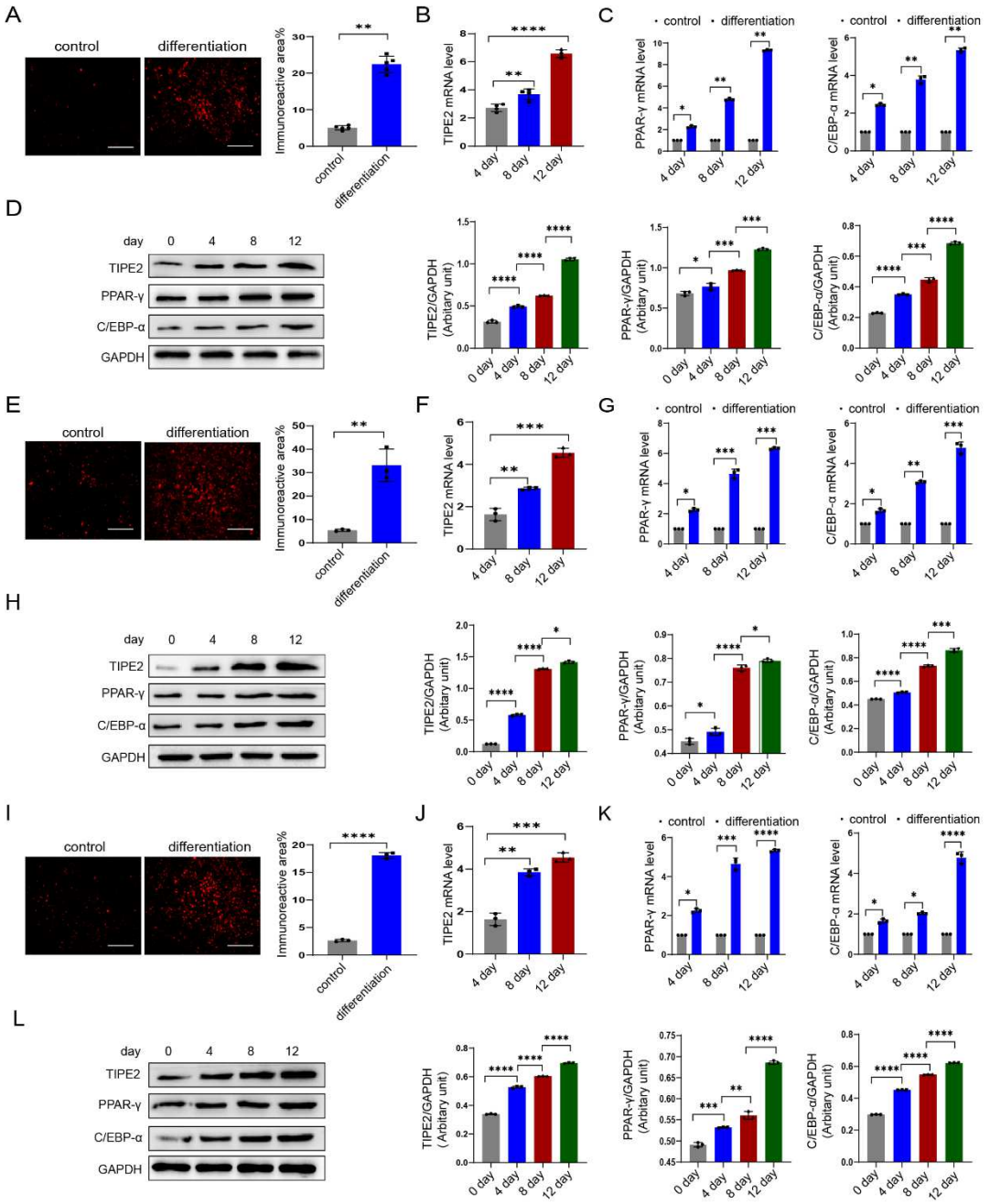


Fig 3 TIPE2 is up-regulated in adipogenic differentiation.

(A, E, I)Representative immunofluorescence images showing lipid droplet accumulation during adipogenic differentiation of 3T3-L1 preadipocytes, human preadipocytes, and mouse preadipocytes (scale bar= 300 μm).

(B, F, J)mRNA expression levels of TIPE2 during adipogenic differentiation.

(C, G, K)mRNA expression levels of lipid-forming markers PPAR-γ and C/EBP-α in the three cell types.

(D, H, L)Protein expression levels of TIPE2, PPAR-γ and C/EBP-α at different stages of differentiation.

Data are presented as mean ± SEM from at least three independent experiments. *P < 0.05, **P < 0.01, ***P < 0.001, ****P < 0.0001.

TIPE2 negatively regulates adipogenic differentiation in adipocytes

To further investigate the role of TIPE2 in adipogenic differentiation, 3T3-L1 preadipocytes were transduced *in vitro* with lentiviral particles to achieve either TIPE2 knockdown (sh-TIPE2) or TIPE2 overexpression (LV-TIPE2). Fluorescent staining of lipid droplets revealed that TIPE2 knockdown significantly promoted lipid accumulation in 3T3-L1 preadipocytes (Figure 4A), conversely, TIPE2 overexpression was accompanied by a marked reduction in 3T3-L1 cells lipid-droplet content (Figure 4B). RT-qPCR and Western blotting results showed that the mRNA and protein levels of PPAR-γ and C/EBP-α were significantly increased after the differentiation of 3T3-L1 preadipocytes infected with sh-TIPE2 (Figures 4C and 4D). The mRNA and protein levels of PPAR-γ and C/EBP-α were significantly decreased after the differentiation of 3T3-L1 preadipocytes infected with LV-TIPE2 (Figures 4E and 4F).

To determine whether the anti-adipogenic effect of TIPE2 is conserved across species, we further examined its role in primary mouse preadipocytes and in human preadipocytes. Similar to the observations in 3T3-L1 cells, TIPE2 knockdown significantly enhanced lipid droplet accumulation and increased PPAR-γ and C/EBP-α expression, whereas TIPE2 overexpression suppressed adipogenic differentiation in both murine and human preadipocyte cells (Figures S3 and S4).

Collectively, these data demonstrate that TIPE2 acts as a conserved negative regulator of adipogenic differentiation across multiple adipocyte models, suggesting a fundamental role for TIPE2 in controlling adipocyte lineage commitment and lipid storage.

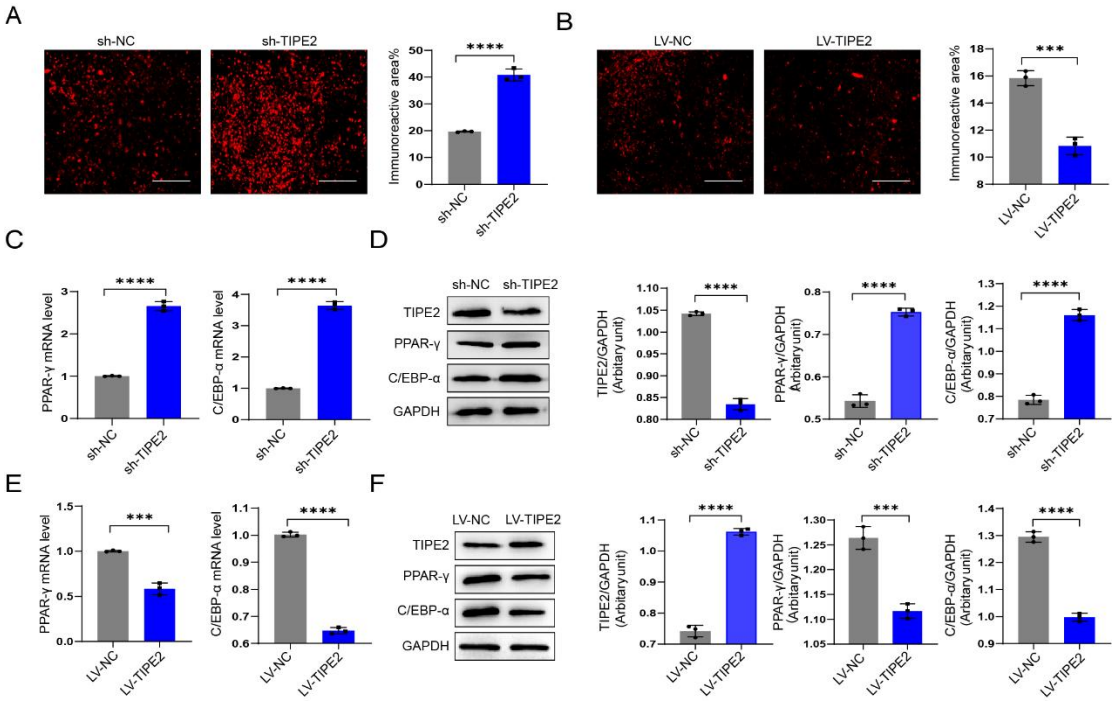


Fig 4 TIPE2 inhibits adipogenic differentiation of 3T3-L1 preadipocytes

(A)Lipid droplet levels in 3T3-L1 preadipocytes after TIPE2 knockdown (scale bar= 300 μm).

(B)Lipid droplet levels in 3T3-L1 preadipocytes after TIPE2 overexpression (scale bar= 300 μm).

(C)The mRNA levels of PPAR-γ and C/EBP-α in 3T3-L1 preadipocytes after TIPE2 knockdown.

(D)Protein expression levels of TIPE2, PPAR-γ and C/EBP-α in 3T3-L1 preadipocytes after TIPE2 knockdown.

(E)The mRNA levels of PPAR-γ and C/EBP-α in 3T3-L1 preadipocytes after TIPE2 overexpression.

(F)Protein expression levels of TIPE2, PPAR-γ and C/EBP-α in 3T3-L1 preadipocytes after TIPE2 overexpression.

Data are presented as mean ± SEM from at least three independent experiments. ***P < 0.001, ****P < 0.0001.

TIPE2 promotes the overall level of m6A methylationin in adipogenic differentiation.

In order to explore whether m6A modification is involved in the regulation of fat differentiation, the EpiQuik m6A RNA methylation quantification kit and m6A dot blot hybridization assay were used to detect the changes in the overall level of m6A methylation. The results showed that in 3T3-L1 preadipocytes, the total m6A methylation level decreased after adipogenic differentiation compared with undifferentiated controls. Methylene blue (MB) staining of total RNA was used as a loading control for the dot blot (Figure 5A). The mRNA levels of m6A modification-related methyltransferases and demethylases were detected. RT-qPCR analysis showed that the mRNA levels of demethylases ALKBH5 and FTO, and methyltransferase METTL3 were significantly increased, while the mRNA levels of methyltransferase METTL14 and WTAP were decreased in differentiated 3T3-L1 cells compared with preadipocytes. (Figure 5B).

The results showed that TIPE2 knockdown decreased total m6A methylation, increased FTO and METTL3 mRNA levels, and decreased METTL14 and WTAP mRNA levels (Figures 5C and 5D). Conversely, TIPE2 overexpression had the opposite effect (Figures 5E and 5F)." . These results suggest that TIPE2 regulates the overall level of m6A methylation and modulates the expression of methyl-modifying enzymes during adipogenic differentiation.

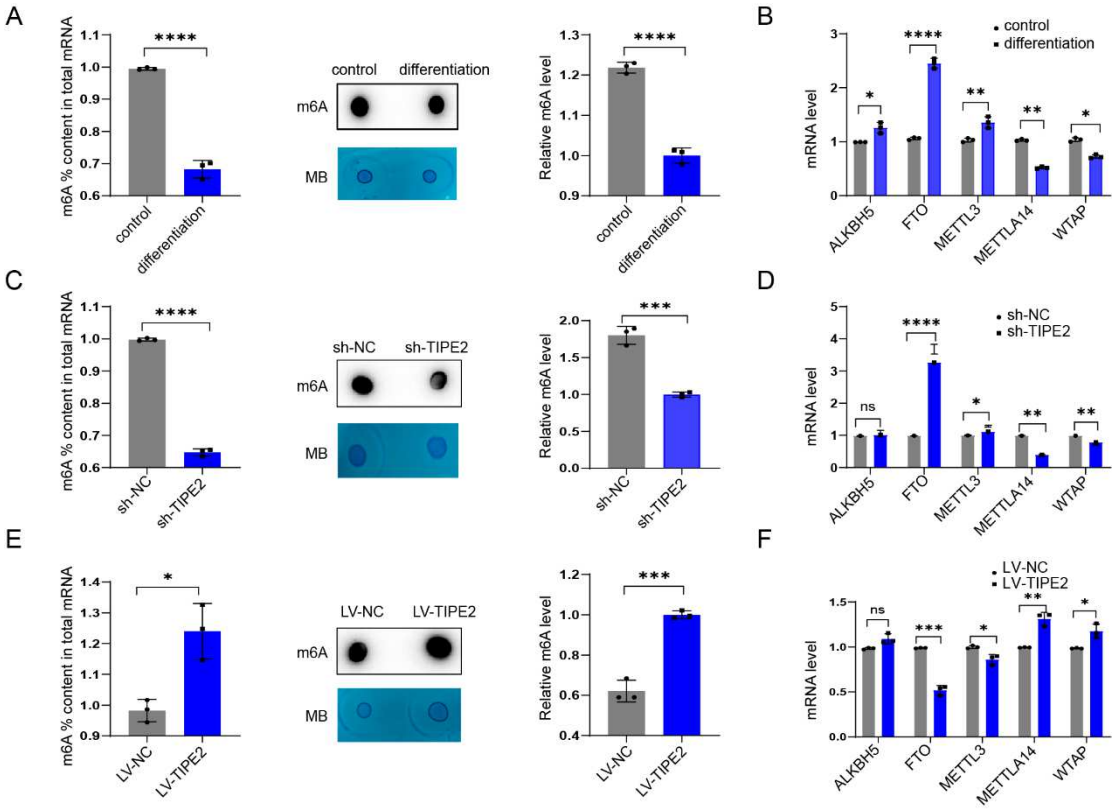


Fig 5 TIPE2 regulates total m6A methylation and the expression of m6A-related enzymes during adipogenic differentiation.

(A)The overall level of m6A methylation in adipogenic differentiation.

(B)The mRNA expression levels of m6A methylation-related enzymes in adipogenic differentiation.

(C)The overall level of m6A methylation after TIPE2 knockdown.

(D)The mRNA expression levels of m6A methylation-related enzymes after TIPE2 knockdown.

(E)The overall level of m6A methylation after TIPE2 overexpression.

(F)The mRNA expression levels of m6A methylation-related enzymes after TIPE2 overexpression.

Data are presented as mean ± SEM from at least three independent experiments. *P < 0.05, **P < 0.01, ***P < 0.001, ****P < 0.0001.

The results of MeRIP-Seq suggest that TIPE2 regulates the m6A levels via METTL14.

To elucidate the role of TIPE2 in m6A regulation, we performed methylated RNA immunoprecipitation sequencing (MeRIP-seq) in 3T3-L1 preadipocytes stably expressing either sh-

TIPE2 or sh-NC (Figure 6A). Loss of TIPE2 did not alter the global distribution pattern of m6A peaks, which were predominantly enriched in the 3′ untranslated region (3′UTR) and near stop codons (Figures 6B and 6C), consistent with canonical m6A topology. Transcriptome analysis identified significant DEGs following TIPE2 knockdown (Figure 6D), and heatmap clustering revealed that genes involved in RNA modification pathways were markedly altered (Figure 6E). Notably, the m6A methyltransferase METTL14 was significantly upregulated upon TIPE2 depletion (highlighted in Figure 6E). To explore potential interacting partners of TIPE2, a STRING-based protein–protein interaction analysis was performed. The TIPE2-centered network revealed a close association with METTL14, suggesting a potential functional link between TIPE2 and the m6A methyltransferase machinery (Figure 6F). To determine whether TIPE2 directly interacts with m6A machinery, we performed co-immunoprecipitation (Co-IP) assays, which confirmed a physical association between TIPE2 and METTL14 (Figure 6G). The structural basis of the METTL14-TIPE2 interaction was elucidated through comparative modeling and protein-protein docking analysis. The tertiary structures of human and murine METTL14 （hMETTL14 and mMETTL14） and TIPE2 proteins(hTIPE2 and mTIPE2) were individually predicted and subsequently subjected to protein-protein docking using AlphaFold3. The docking results revealed conserved interaction patterns between the orthologous proteins from different species (Figure 6H). In the murine complex, key interacting residues including His116, Arg135, Glu136, Phe139, and Gly142 of METTL14 formed interactions with Arg58, Glu79, Lys138, Glu78, Asp75, and Lys20 of TIPE2 (Figure 6I). Similarly, the human complex exhibited analogous interaction interfaces, with critical residues such as Phe109, Glu112, Thr110, Glu96, Thr295, Lys69, Arg89, Gln92, Asp24, Asp180, and Arg255 participating in the binding (Figure 6J). These structural analyses demonstrate that the METTL14-TIPE2 interaction is mediated by specific amino acid residues at the interface, forming a stable complex through hydrogen bonding and hydrophobic interactions. The conservation of these interaction patterns across species suggests an evolutionarily conserved mechanism of METTL14-TIPE2 complex formation, which may play a crucial role in their functional regulation.

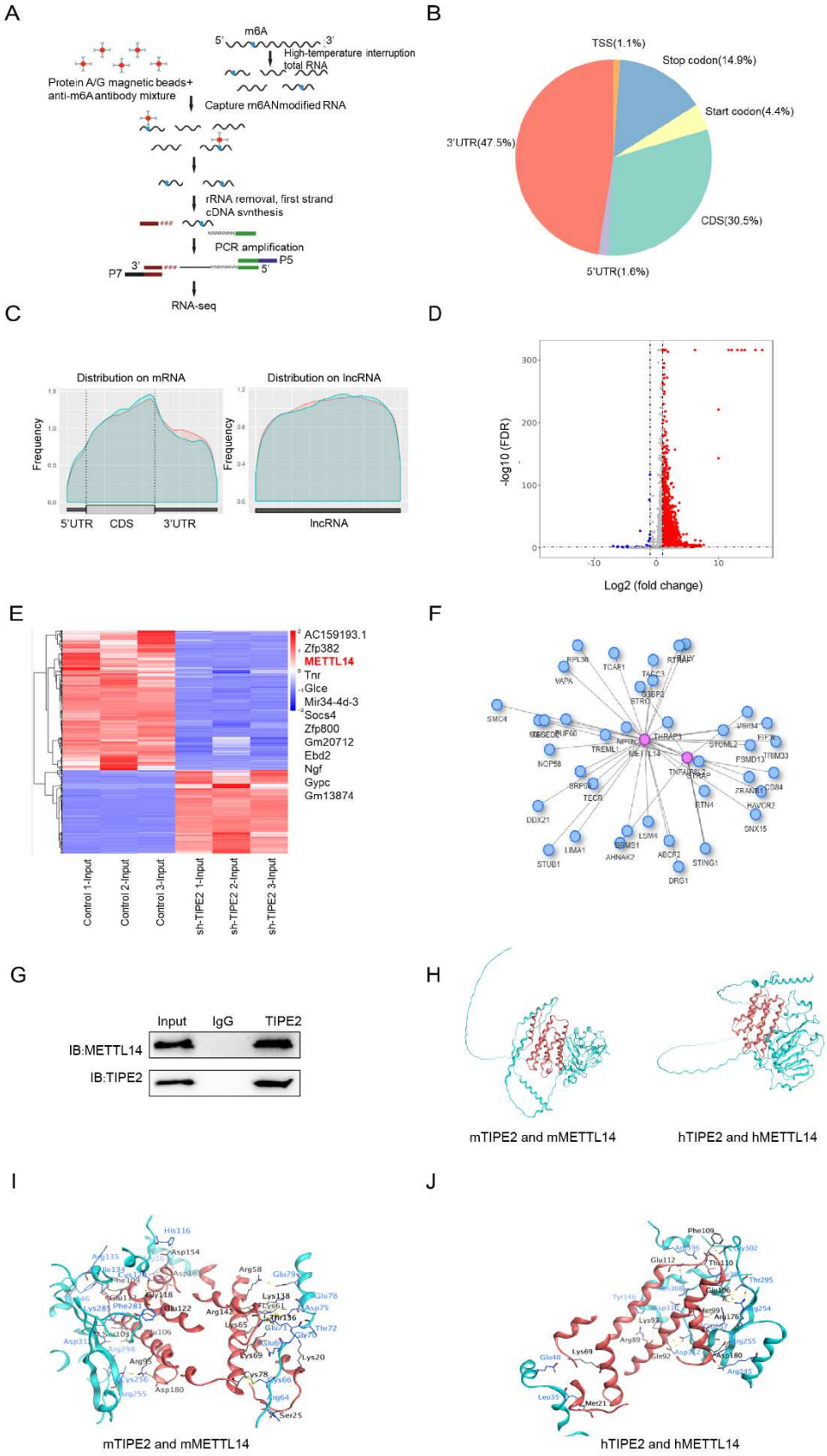


Fig 6 TIPE2 regulated the m6A levels via METTL14

(A)Experimental flow chart of MeRIP-seq.

(B)Pie plot of Peak's distribution on RNA structure.

(C)Metagene profile showing m6A peak enrichment across mRNA and lncRNA transcripts.

(D)Volcano plot of DEGs following TIPE2 knockdown in 3T3-L1 preadipocytes.

(E)Heatmap of DEGs, including significantly altered RNA-modifying enzymes, with METTL14 highlighted.

(F)STRING PPI analysis identified METTL14 as a potential TIPE2-interacting protein.

(G)Co-IP experiments showed the interaction between TIPE2 and METTL14.

(H)AlphaFold3-predicted docking models of METTL14-TIPE2 complexes from mouse (left) and human (right) species.

(I)The interaction residue analysis of mMETTL14 and mTIPE2 was conducted using AlphaFold3-predicted docking models.

(J)The interaction residue analysis of hMETTL14 and hTIPE2 was conducted using AlphaFold3-predicted docking models.

METTL14 is positively regulated by TIPE2, and is a downstream regulator of TIPE2 associated adipogenic differentation.

Next, to further elucidate the relationship between TIPE2 and METTL14, we evaluated the expression of METTL14 by altering the expression level of TIPE2. Western blotting results showed that METTL14 expression decreased after TIPE2 knockdown (Figure 7A), and increased after TIPE2 overexpression (Figure 7B). The immunoblotting results showed that, compared with control mice, METTL14 expression was markedly decreased in both subcutaneous and visceral adipose tissues of Tipe2$^{-/-}$ mice, whereas the adipogenic transcription factors PPAR-γ and C/EBP-α were significantly upregulated (Figure 7C). Consistently, immunohistochemical staining further confirmed reduced METTL14 expression in adipose tissues from *Tipe2*$^{-/-}$ mice relative to WT controls (Figure 7D). Similar expression patterns were observed in human adipose samples, in which decreased TIPE2 levels were associated with lower METTL14 and higher PPAR-γ and C/EBP-α expression (Figure 7E). These results suggest that METTL14 is positively regulated by TIPE2. To further investigate the role of METTL14 in TIPE2-mediated adipogenesis, we constructed METTL14 overexpressing lentivirus (LV-METTL14) for subsequent experiments. Fluorescent lipid droplet staining showed that overexpression of METTL14 reduced the lipid accumulation (Figure 7F) in TIPE2-knockdown cells, and METTL14 overexpression significantly decreased the mRNA and protein levels of PPAR-γ and C/EBP-α in TIPE2-knockdown cells (Figures 7G and 7H), demonstrating that METTL14 partially rescues the pro-adipogenic effects in TIPE2 associated effects of adipogenic differentiation. Importantly, the same rescue effects were observed in mouse primary preadipocytes and human preadipocytes, in which METTL14 overexpression similarly suppressed lipid accumulation and adipogenic gene expression in TIPE2-knockdown cells (Figure S5), indicating that the TIPE2–METTL14 axis is conserved across species and functions as a central checkpoint in adipogenic differentiation.

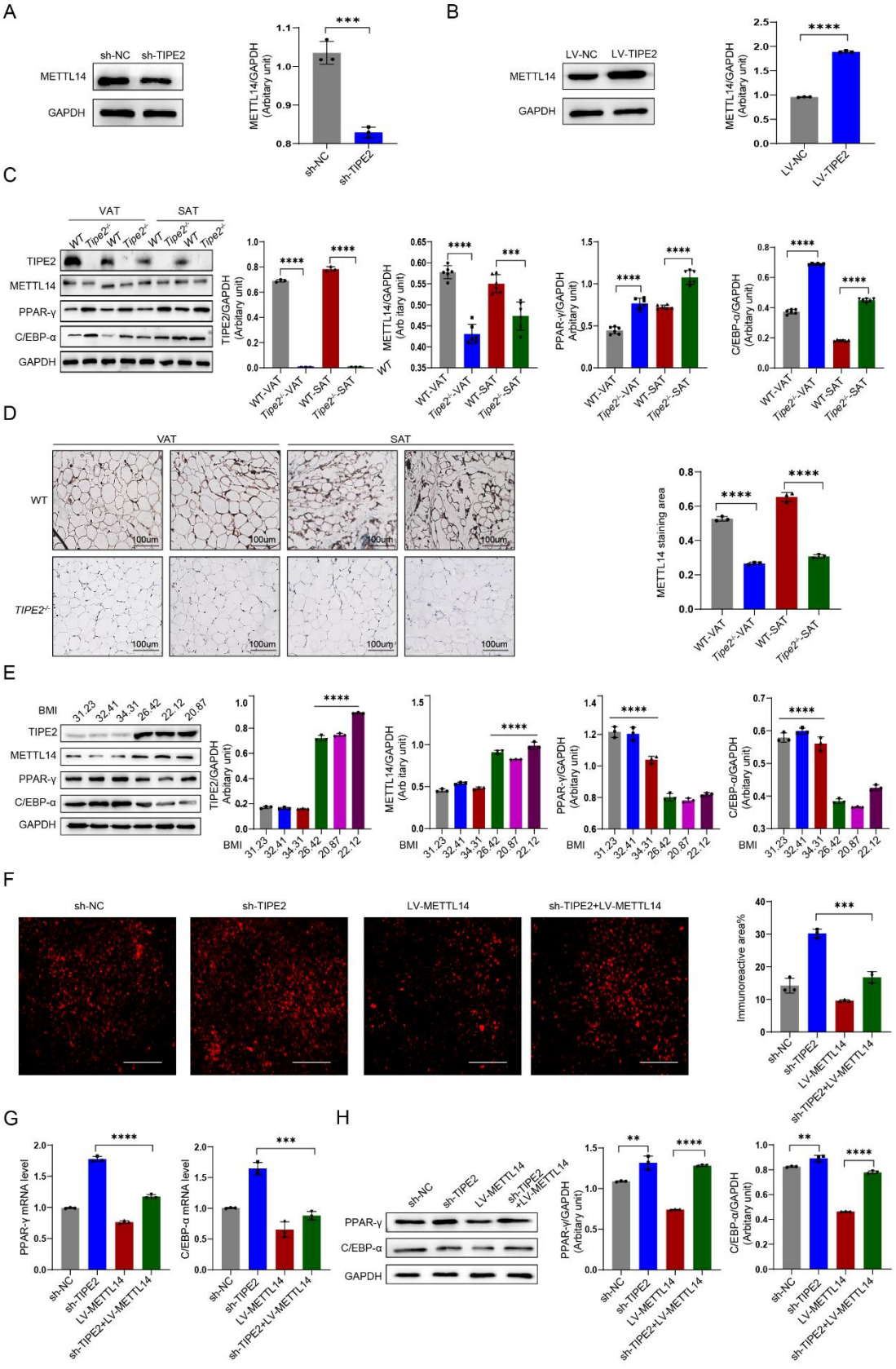


Fig 7 TIPE2 positively regulates METTL14.

(A)Protein expression of METTL14 in 3T3-L1 preadipocytes after TIPE2 knockdown.

(B)Protein expression of METTL14 in 3T3-L1 preadipocytes after TIPE2 overexpression.

(C)The protein expression levels of METTL14, PPAR-γ and C/EBP-α in VAT and subcutaneous adipose tissue (SAT) of *Tipe2*$^{-/-}$ and WT mice.

(D)Immunohistochemical analysis of METTL14 in adipose tissues from *Tipe2*$^{-/-}$ and WT mice (scale bar= 100 μm).

(E)The protein expression levels of METTL14, PPAR-γ and C/EBP-α in human preadipocytes.

(F)Representative images of fluorescent lipid droplet staining (scale bar= 300 μm).

(G)The mRNA expression levels of PPAR-γ and C/EBP-α following modulation of TIPE2 and METTL14 expression.

(H)The expression levels of PPAR-γ and C/EBP-α proteins following modulation of TIPE2 and METTL14 expression.

Data are presented as mean ± SEM from at least three independent experiments. **P < 0.01, ***P < 0.001, ****P < 0.0001.

Restoration of TIPE2 alleviates obesity and metabolic dysfunction in obese mice

To determine whether restoring TIPE2 expression is sufficient to reverse obesity-associated metabolic abnormalities, HFD–induced obese mouse model was established. Mice were intravenously injected with adeno-associated virus encoding TIPE2 (AAV-TIPE2) or adeno-associated virus encoding GFP (AAV-GFP) via the tail vein (Figure 8A). Consistent with a protective metabolic role of TIPE2, HFD-fed mice receiving AAV-TIPE2 exhibited a significantly attenuated body-weight gain compared with AAV-GFP controls (Figure 8B).

TIPE2 overexpression markedly reduced the mass of epididymal VAT and SAT (Figures 8C and 8D). Hematoxylin and Eosin staining (H&E) staining demonstrated that adipocyte hypertrophy was markedly alleviated in mice treated with AAV-TIPE2, as evidenced by a clear reduction in adipocyte size and confirmed by quantitative analysis of adipocyte area (Figure 8E). At the systemic metabolic level, AAV-TIPE2 treatment significantly reduced circulating TG and TC levels, indicating improved lipid metabolism (Figure 8F).

Metabolic tolerance tests were performed to evaluate glucose homeostasis and insulin sensitivity. OGTT showed that TIPE2 restoration significantly decreased blood glucose levels and reduced the AUC (Figure 8G). Similarly, ITT and AUC analysis demonstrated that TIPE2 overexpression markedly improved insulin sensitivity (Figure 8H). Consistent with these findings, TIPE2 restoration significantly decreased the HOMA-IR index and circulating resistin levels, indicating an overall improvement in systemic insulin sensitivity (Figures 8I and 8J).

Mechanistically, restoration of TIPE2 significantly upregulated the expression of METTL14 in adipose tissue while suppressing the adipogenic transcription factors PPAR-γ and C/EBP-α at protein levels. (Figure 8K) Immunohistochemical staining further confirmed increased METTL14 expression in adipose tissue from AAV-TIPE2–treated mice (Figure 8L), consistent with the molecular findings.

Collectively, these findings demonstrate that restoration of TIPE2 is sufficient to alleviate obesity and metabolic dysfunction *in vivo*, highlighting a critical role of TIPE2 in maintaining energy homeostasis and regulating glucose metabolism, possibly through modulation of the METTL14–PPAR-γ signaling axis.

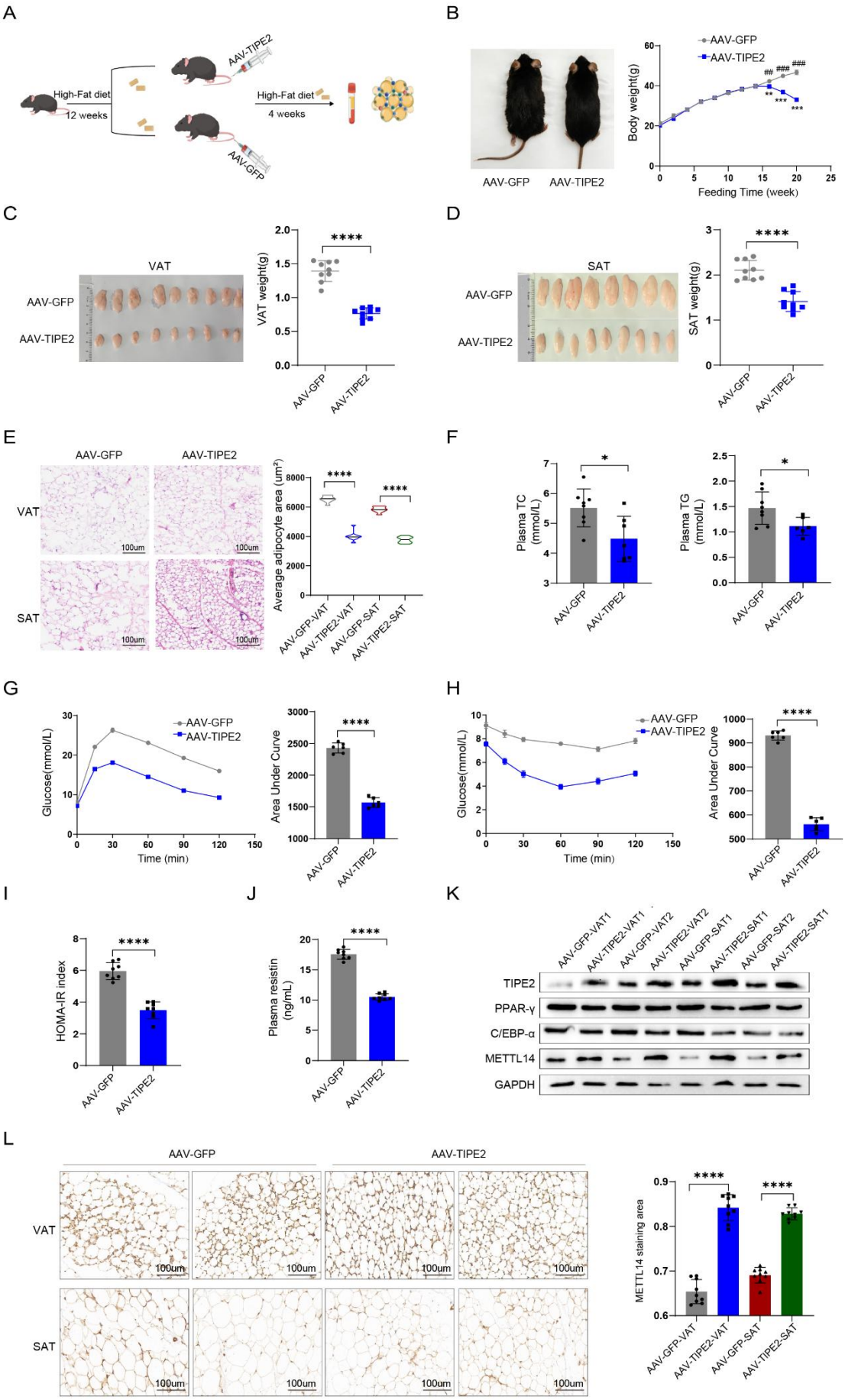

A
High-Fat diet
12 weeks
AAV-TIPE2
AAV-GFP
High-Fat diet
4 weeks
B
AAV-GFP
AAV-TIPE2
Body weight(g)
Feeding Time (week)
C
VAT
AAV-GFP
AAV-TIPE2
VAT weight(g)
D
SAT
SAT weight(g)
E
AAV-GFP
AAV-TIPE2
VAT
SAT
100um
Average adipocyte area (um²)
AAV-GFP-VAT
AAV-TIPE2-VAT
AAV-GFP-SAT
AAV-TIPE2-SAT
F
Plasma TC (mmol/L)
Plasma TG (mmol/L)
G
Glucose(mmol/L)
Time (min)
Area Under Curve
H
I
HOMA-IR index
J
Plasma resistin (ng/mL)
K
AAV-GFP-VAT1
AAV-TIPE2-VAT1
AAV-GFP-VAT2
AAV-TIPE2-VAT2
AAV-GFP-SAT1
AAV-TIPE2-SAT1
AAV-GFP-SAT2
AAV-TIPE2-SAT2
TIPE2
PPAR-γ
C/EBP-α
METTL14
GAPDH
L
METTL14 staining area

Fig 8 TIPE2 restoration alleviates obesity and metabolic dysfunction in HFD-fed mice via the METTL14–PPAR-γ axis.

(A) Schematic diagram of the experimental design showing AAV-TIPE2 or AAV-GFP administration in HFD-induced obese mice.

(B) Body weight changes in HFD-fed mice following AAV-TIPE2 or AAV-GFP treatment (n=9).

(C, D) Representative images and quantitative analysis of VAT and SAT mass (n=9).

(E) Representative H&E staining of adipose tissue, along with quantitative analysis of adipocyte area (scale bar= 100 μm).

(F) TG and TC levels (n=8).

(G) OGTT curves and corresponding AUC analysis (n=6).

(H) ITT curves and corresponding AUC analysis (n=6).

(I, J) HOMA-IR index and circulating resistin levels (n=8).

(K) The protein expression levels of TIPE2, METTL14, PPAR-γ and C/EBP-α in VAT and SAT of AAV-TIPE2 and AAV-GFP mice.

(L) Immunohistochemical staining of METTL14 in adipose tissue (scale bar= 100 μm).

All data are expressed as mean ± SEM. *P < 0.05, ****P < 0.0001.

PPAR-γ is a downstream effector of the TIPE2-METTL14-m6A adipogenic differentiation pathway

PPAR-γ is a member of the nuclear receptor superfamily and has been shown to regulate terminal adipogenic differentiation. To further confirm whether TIPE2 regulates adipogenic differentiation through the PPAR-γ pathway, we performed gain- and loss-of-function experiments in 3T3-L1 preadipocytes, combined with pharmacological activation or inhibition of PPAR-γ. In the TIPE2 knockdown group, co-treatment with the PPAR-γ inhibitor T0070907 (10 μM, added from day 0 to day 6 of differentiation) significantly reduced lipid accumulation, effectively abolishing the pro-adipogenic effect of TIPE2 silencing (Figure 9A). RT-qPCR analysis confirmed that adipogenic marker genes were significantly upregulated upon TIPE2 knockdown, which was blocked by T0070907 treatment (Figure 9B). Western blot analysis further revealed that TIPE2 knockdown upregulated PPAR-γ and C/EBP-α protein levels, while T0070907 treatment suppressed their expression (Figure 9C). In the TIPE2 overexpression group, treatment with the PPAR-γ agonist rosiglitazone (1 μM, from day 0 to day 6 of differentiation) partially rescued the effect of TIPE2 overexpression, resulting in increased lipid deposition (Figure 9D). RT-qPCR analysis confirmed that lipid content was significantly

decreased in TIPE2-overexpressing cells, and rosiglitazone treatment restored lipid accumulation (Figure 9E). Consistently, Western blot analysis showed that TIPE2 overexpression reduced the levels of PPAR-γ and C/EBP-α, while rosiglitazone reversed these changes (Figure 9F).

To validate the universality of this regulatory axis, we further examined the effects of TIPE2–PPAR-γ modulation in mouse primary preadipocytes and human preadipocytes. Similar to 3T3-L1 cells, TIPE2 knockdown enhanced adipogenic differentiation in both murine and human preadipocyte cells, which was abolished by T0070907, whereas TIPE2 overexpression suppressed adipogenesis, which was partially rescued by rosiglitazone (Figure S6). These data indicate that the TIPE2–PPAR-γ regulatory axis is conserved across species.

Collectively, these results demonstrate that TIPE2 regulates adipogenic differentiation through the PPAR-γ signaling pathway, acting downstream of the TIPE2–METTL14–m6A axis. TIPE2 deficiency promotes adipogenesis via PPAR-γ activation, whereas TIPE2 overexpression suppresses adipogenic differentiation by inhibiting PPAR-γ activity.

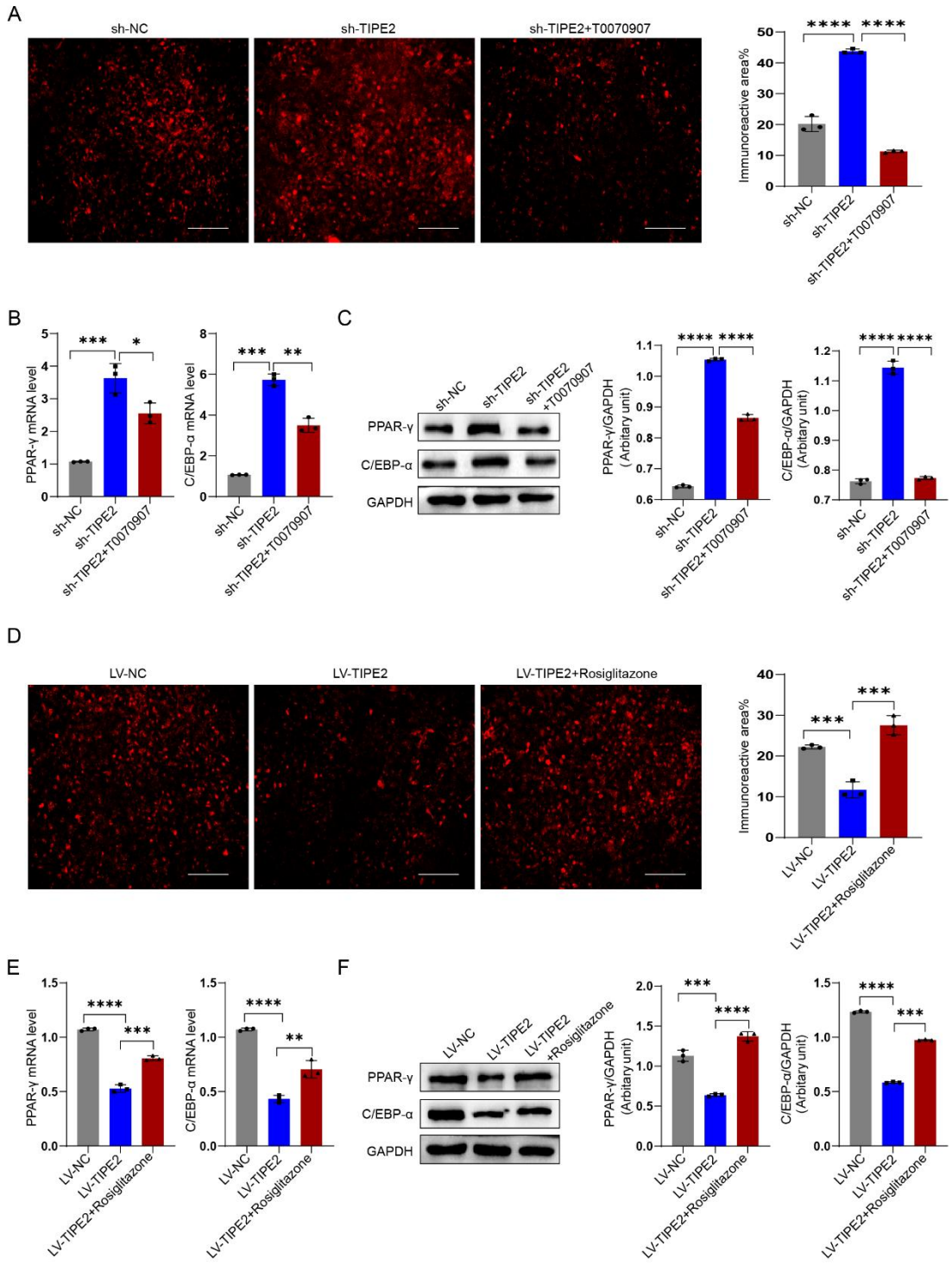


Fig 9 TIPE2 suppresses adipogenesis in 3T3-L1 preadipocytes via modulation of the PPAR-γ pathway.

(A)Representative images of fluorescent lipid droplet staining in 3T3-L1 preadipocytes with TIPE2 knockdown in the presence or absence of the PPAR-γ inhibitor T0070907 (scale bar = 300 μm).

(B)The mRNA expression levels of PPAR-γ and C/EBP-α.

(C)The protein expression levels of PPAR-γ and C/EBP-α in 3T3-L1 preadipocytes following treatment with the PPAR-γ inhibitor T0070907.

(D)Representative images of fluorescent lipid droplet staining in 3T3-L1 preadipocytes with TIPE2 overexpression in

the presence or absence of the PPAR-γ agonist rosiglitazone (scale bar = 300 μm).

(E)The mRNA expression levels of PPAR-γ and C/EBP-α in 3T3-L1 preadipocytes following treatment with the PPAR-γ agonist rosiglitazone.

(F)The protein expression levels of C/EBP-α and PPAR-γ in 3T3-L1 preadipocytes following treatment with the PPAR-γ agonist rosiglitazone.

All data are expressed as mean ± SEM from at least three independent experiments. *P < 0.05, **P < 0.01, ***P < 0.001, ****P < 0.0001.

Conclusions

This study reveals a critical role for TIPE2 in coordinating adipogenesis and metabolic homeostasis, and proposes a mechanistic model integrating immune-metabolic crosstalk in obesity.

TIPE2 acts as a negative regulator in maintaining immune homeostasis in both innate and adaptive immunity[19]. Abnormal expression of TIPE2 has been found in some immune-related diseases, highlighting its potential as a therapeutic target for inflammatory diseases[20]. The multiple functions demonstrated by the TIPE protein family, particularly the regulatory role of TIPE2, suggest that these proteins have important potential in the treatment of related diseases. Previous studies have demonstrated that TIPE2 plays an important role in metabolism[21,22]. Recent studies have shown that overexpression of TIPE2 promotes the viability and migration of adipose-derived stem cells (ADSCs) by activating Toll-like receptor 4–extracellular signal-regulated kinase 1/2 signaling pathway, and that ADSCs transfected with TIPE2 inhibit the abnormal proliferation and apoptosis of damaged pulmonary smooth muscle cells through NF-κB signaling, and promote the transformation of pulmonary smooth muscle cells from synthesis to contraction[23]. TIPE2 expression was upregulated in the liver under fasting conditions and was positively correlated with the expression of gluconeogenic genes. During prolonged fasting, liver TIPE2 deficiency leads to abnormal activation of the ERK-mTORC1 axis, thereby increasing liver fat accumulation through lipid production[21].

Adipose tissue is composed not only of adipocytes but also immune cells and stromal components, whose interactions determine tissue function and metabolic health[24,25]. Obesity is characterized by increased infiltration and functional dysregulation of adipose tissue macrophages (ATMs), which serve as key drivers of chronic low-grade inflammation and metabolic dysfunction[26,27]. Recent work by Tao et al. demonstrated that obesity-associated

ATMs propagate fragmented mitochondrial signals and ferroptotic stress to neighboring adipose stem cells (ASCs), impairing ASC viability, limiting adipose tissue regenerative capacity, and shifting adipose expansion from hyperplasia to pathological hypertrophy[28]. Integrating these findings with our data, TIPE2 appears to coordinate a dual-cell protective mechanism within adipose tissue: in preadipocytes/adipocytes, TIPE2 acts as a "quality control factor," maintaining METTL14-mediated m6A methylation to restrain PPAR-γ/C/EBP-α activity.

Lipid metabolism is a complex process, and the regulation of lipid metabolism involves a variety of cell signaling pathways and mechanisms[29,30]. In recent years, the role of m6A modification in lipid metabolism has become a research focus. m6A is one of the post-transcriptional modifications of mRNA, and a large number of studies have proved that m6A modification plays an important role in lipid metabolism[31-33]. Studies have found that METTL3 can regulate lipid accumulation by making the mRNA of metabolism-related genes more unstable through mediated m6A methylation, leading to metabolic disorders and lipid accumulation in the liver[34]. Similarly, in cardiomyocytes, METTL3 deficiency reduces m6A methylation levels, leading to the accumulation of triglycerides[34]. Emerging evidence suggests that FTO can regulate lipid metabolism through the m6A demethylation modification process[35,36].

In the context of our findings, the observation that the pro-adipogenic effect of TIPE2 knockdown was completely abrogated by the PPAR-γ inhibitor T0070907 places PPAR-γ squarely downstream of the TIPE2-METTL14 axis. This suggests that the suppression of adipogenesis by TIPE2 is ultimately mediated through the attenuation of PPAR-γ signaling activity. Our data contribute to the evolving understanding that upstream regulators, including epigenetic modifiers like METTL14, converge upon this central transcription factor to fine-tune adipogenic capacity and lipid storage.

We chose to prioritize the PPAR-γ pathway because it represents the master transcriptional regulator of adipogenic differentiation and lipid storage, and because both our phenotypic and mechanistic data converged strongly on this axis. Specifically, TIPE2 knockdown enhanced lipid accumulation, a phenotype that was nearly completely abolished by pharmacological inhibition of PPAR-γ. METTL14 overexpression also rescued the adipogenic effect caused by TIPE2 depletion, further suggesting that the TIPE2–METTL14–PPAR-γ node

constitutes a dominant regulatory module. While additional m6A-dependent targets are likely to contribute, our data indicate that modulation of PPAR-γ signaling is the most proximal and functionally consequential pathway mediating the effects of TIPE2 in adipogenic differentiation.

Based on these findings, we propose a mechanistic model in which TIPE2 suppresses adipogenic differentiation through activation of METTL14-dependent m6A modification and subsequent inhibition of PPAR-γ signaling, thereby limiting lipid accumulation and obesity-associated metabolic dysfunction (Figure 10).

Therapeutically, restoring TIPE2 activity may provide dual benefits. In adipocyte lineages, reactivation of the TIPE2–METTL14–m6A–PPAR-γ axis could fine-tune adipogenesis and prevent pathological lipid accumulation. In ATMs, restoring TIPE2 or blocking its downstream effects-such as mitochondrial fragmentation and dysregulated iron handlin-may protect ASCs and support healthy adipose tissue regeneration. Small molecules or gene modulation strategies aimed at enhancing TIPE2 expression or mimicking its regulatory functions may be particularly effective if applied in a tissue- or cell type-specific manner.

Future studies should delineate depot-specific roles of TIPE2 in subcutaneous versus visceral fat, define its interaction with critical metabolic pathways such as insulin signaling and AMPK, and leverage single-cell and spatial multi-omics approaches to map TIPE2-dependent intercellular circuits in human adipose tissues. These investigations will inform the development of multi-target strategies that exploit TIPE2's regulatory capacity to combat obesity and associated metabolic diseases.

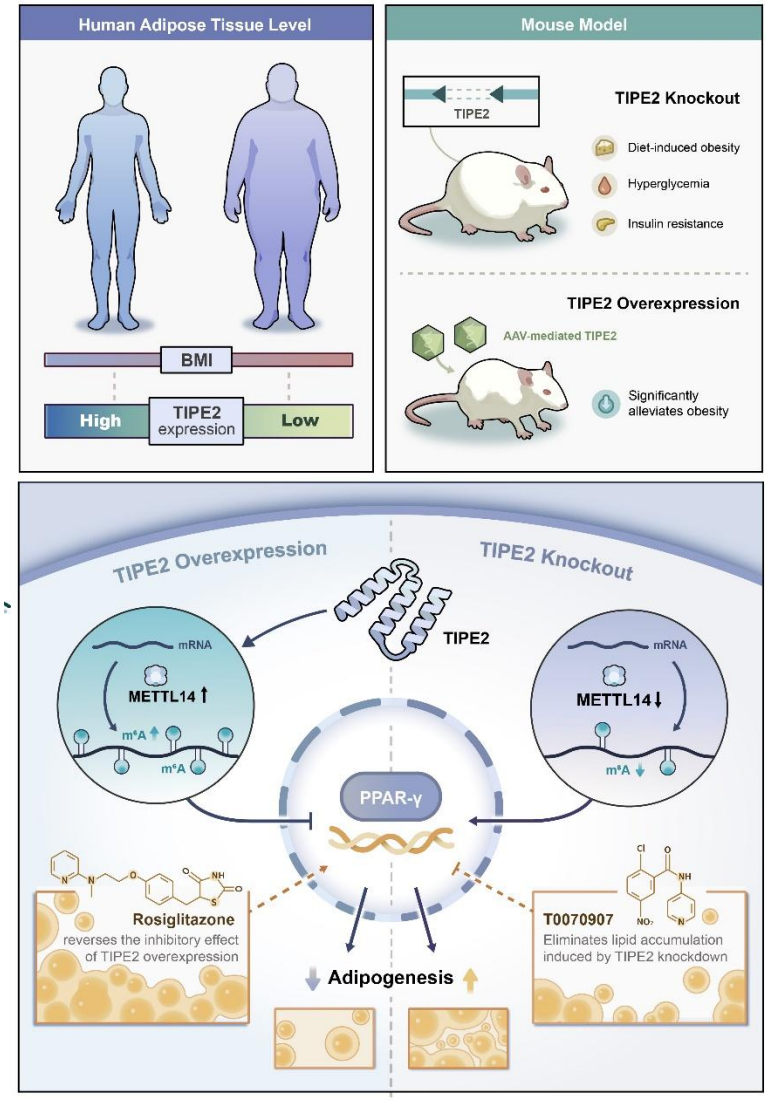


Fig 10. The protective role of TIPE2 in adipose tissue homeostasis and obesity.

TIPE2 upregulates METTL14 expression and m6A modification, thereby suppressing PPAR-γ signaling and adipogenic differentiation. In parallel, TIPE2 may regulate adipose tissue macrophage function and adipose stem cell homeostasis, contributing to healthy adipose tissue remodeling and metabolic balance. Loss of TIPE2 promotes adipogenesis, lipid accumulation, and obesity-associated metabolic dysfunction.

Collectively, these studies have established TIPE2 as an important regulator of immune homeostasis and metabolic adaptation. Our findings substantially extend this concept by demonstrating that TIPE2 also functions as a negative regulator of adipogenic differentiation. Unlike previous studies that primarily focused on hepatic glucose and lipid metabolism or stem cell function, our work identifies adipocyte differentiation as an additional biological process regulated by TIPE2 and provides mechanistic evidence linking TIPE2 to METTL14-dependent m6A modification.

Limitations and future work

In this study, we identify TIPE2 as a critical regulator of METTL14-dependent m6A signaling during adipogenesis and metabolic regulation. Nonetheless, several limitations should be noted. First, although we establish a physical interaction between TIPE2 and METTL14, the precise molecular interface and structural determinants underlying this interaction remain undefined. Future studies applying systematic mutagenesis together with structural biology techniques, such as cryo-EM or X-ray crystallography, will be required to delineate the specific domains and residues that mediate TIPE2–METTL14 binding. Second, although gene-based modulation of metabolic regulators is an emerging therapeutic concept, strategies aimed at targeting TIPE2 remain at an early developmental stage. Approaches such as viral-mediated gene delivery, CRISPR activation platforms, or nanoparticle-based nucleic acid delivery could, in principle, alter TIPE2 expression. However, these technologies currently face significant barriers—including limited tissue specificity, suboptimal delivery efficiency, long-term safety concerns, and potential immunogenicity that must be addressed before TIPE2-directed interventions can be realistically considered for translational or clinical applications. Third, our mechanistic investigation of TIPE2 in adipogenesis was mainly performed in 3T3-L1 preadipocytes. Although the key phenotypes were validated in both human and mouse preadipocytes, mechanistic gain- and loss-of-function studies were not conducted in these primary cells. Future studies using lineage-specific genetic models or advanced primary cell systems are needed to further strengthen the physiological and translational relevance of our findings.

Acknowledgements: The authors would like to thank all members, for their valuable discussions, technical assistance, and support throughout this study. We also acknowledge the support provided by the Experimental Research Center for animal experiments, molecular biology analyses, and instrument access.

CRediT authorship contribution statement: Chuanjie Liang: Conceptualization, Methodology, Investigation, Formal analysis, Data curation, Writing-Original draft. **Yangjunjie Wang:** Investigation, Methodology, Validation, Data curation. **Wenxiang Zheng:** Investigation, Visualization. **Wenxiu Tian:** Investigation. **Chuanqin Shi:** Investigation. **Tianchu Li:** Investigation. **Wing-Kin Syn:** Supervision, Writing-Review & Editing. **Patricia Aspichueta:** Supervision, Writing-Review & Editing. **Xiaodong Zhao:** Conceptualization, Funding

acquisition, Supervision, Writing-Review & Editing. **Wei Hou:** Conceptualization, Funding acquisition, Project administration, Supervision, Writing-Review & Editing. **Xinxin Xiang:** Conceptualization, Funding acquisition, Project administration, Supervision, Writing-Review & Editing.

Funding sources: This study was supported by the Shandong Provincial Natural Science Foundation Joint Fund for Innovative Development (ZR2025LSW013), the Natural Science Foundation of Shandong Province (ZR2024MH344, ZR2024QC222, ZR2025MS1275 and ZR2025MS1395), the Shandong Province Traditional Chinese Medicine Project (Z20240306 and M20250303), Qilu Medical University High-Level Talent Research Startup Fund (X2024BSJJ020), Shandong Medical and Health Science & Technology Program (202503030929), Zibo Municipal Medical and Health Scientific Research Program (20240309031 and 20240306019), Chronic Disease Management Research Project of National Health Commission Capacity Building and Continuing Education Center (GWJJMB202510025173), Shandong Provincial Key Laboratory of Medical Sciences and the Youth Science and Innovation Team Project.

Ethical Approval: Human subcutaneous adipose tissue samples were obtained from patients undergoing elective liposuction surgery at Zibo Central Hospital. The collected adipose tissue represented surgical waste and was used exclusively for scientific research. The requirement for written informed consent was waived by the Ethics Committee of Zibo Central Hospital Affiliated to Shandong Medical University because sample collection involved no additional intervention and did not affect patient privacy. The study was approved by the Ethics Committee of Zibo Central Hospital Affiliated to Shandong Medical University (Approval No. 20250261).

Declaration of competing interes: The authors declare no competing interests.

Data availability Statement: Refer to Supplementary Information for the patients' information (table 1), key reagents (table 2), antibodies (table 2), primer sequences for RT-qPCR (table 2). The data presented in the study are not publicly available. However, the data can be made available from the corresponding author on a reasonable request.

REFERENCES

1. Lingvay, I.; Cohen, R. V.; Roux, C. W. l.; Sumithran, P. Obesity in adults. *The Lancet* **2024**,

404, 972-987.

2. Chen, X. H.; Guo, K. X.; Li, J.; Xu, S. H.; Zhu, H.; Yan, G. R. Regulations of m(6)A and other RNA modifications and their roles in cancer. *Front Med* **2024**, *18*, 622-648.

3. Dai, G.; Huang, S.; Li, Y.; Tu, X.; Xia, J.; Zhou, Z.; Chen, W.; Zhang, A.; Lin, J.; Li, Y.; He, D.; Lin, T.; Cong, J.; Lei, Y.; Han, L.; Yao, Z.; Liu, W.; Zhou, Y.; Li, Q.; Li, J.; Zhang, Y.; Wu, A.; Xiao, D.; Wang, W.; Zhao, W.; Jia, J.; Lin, X. Mettl3-mediated m(6)A modification plays a role in lipid metabolism disorders and progressive liver damage in mice by regulating lipid metabolism-related gene expression. *Aging (Albany NY)* **2023**, *15*, 5550-5568.

4. DiSpirito, J. R.; Mathis, D. Immunological contributions to adipose tissue homeostasis. *Semin Immunol* **2015**, *27*, 315-321.

5. Duan, X.; Yang, L.; Wang, L.; Liu, Q.; Zhang, K.; Liu, S.; Liu, C.; Gao, Q.; Li, L.; Qin, G.; Zhang, Y. m6A demethylase FTO promotes tumor progression via regulation of lipid metabolism in esophageal cancer. *Cell Biosci* **2022**, *12*, 60.

6. Gao, J.; Zhang, H.; Zhang, F. Research progress of TIPE2 in immune-related diseases. *Int Immunopharmacol* **2023**, *121*, 110514.

7. Gerstner, M.; Heller, V.; Fechner, J.; Hermann, B.; Wang, L.; Lausen, J. Prmt6 represses the pro-adipogenic Ppar-gamma-C/ebp-alpha transcription factor loop. *Sci Rep* **2024**, *14*, 6656.

8. Grootaert, M. O. J.; Bennett, M. R. Vascular smooth muscle cells in atherosclerosis: time for a re-assessment. *Cardiovasc Res* **2021**, *117*, 2326-2339.

9. Guria, S.; Hoory, A.; Das, S.; Chattopadhyay, D.; Mukherjee, S. Adipose tissue macrophages and their role in obesity-associated insulin resistance: an overview of the complex dynamics at play. *Biosci Rep* **2023**, *43*.

10. Hu, Y.; Feng, Y.; Zhang, L.; Jia, Y.; Cai, D.; Qian, S. B.; Du, M.; Zhao, R. GR-mediated FTO transactivation induces lipid accumulation in hepatocytes via demethylation of m(6)A on lipogenic mRNAs. *RNA Biol* **2020**, *17*, 930-942.

11. Islam, A.; Sultana, H.; Nazmul Hassan Refat, M.; Farhana, Z.; Abdulbasah Kamil, A.; Meshbahur Rahman, M. The global burden of overweight-obesity and its association with economic status, benefiting from STEPs survey of WHO member states: A meta-analysis. *Prev Med Rep* **2024**, *46*, 102882.

12. Li, F.; Zhu, X.; Yang, Y.; Huang, L.; Xu, J. TIPE2 Alleviates Systemic Lupus Erythematosus Through Regulating Macrophage Polarization. *Cell Physiol Biochem* **2016**, *38*, 330-339.

13. Li, J.; He, X.; Liu, F.; Zheng, X.; Jiang, J. Tumor Necrosis Factor-alpha-Induced Protein-8-like 2 Transfected Adipose-Derived Stem Cells Regulated the Dysfunction of Monocrotaline Pyrrole-Induced Pulmonary Arterial Smooth Muscle Cells and Pulmonary Arterial Endothelial Cells. *J Cardiovasc Pharmacol* **2024**, *83*, 73-85.

14. Li, R.; Guo, Z. TIPE2: a novel regulatory factor for cardiovascular-related diseases. *J Mol Med (Berl)* **2025**, *103*, 913-921.

15. Li, T.; Wang, W.; Gong, S.; Sun, H.; Zhang, H.; Yang, A. G.; Chen, Y. H.; Li, X. Genome-wide analysis reveals TNFAIP8L2 as an immune checkpoint regulator of inflammation and metabolism. *Mol Immunol* **2018**, *99*, 154-162.

16. Liu, Y.; Huang, X.; Sang, L.; Zhang, Y.; Cao, J.; Kong, Q. Modulation and Reprogramming of Adipose Tissue Macrophages in Obesity. *Biomolecules* **2026**, *16*.

17. Liu, Y.; Sun, Z.; Gui, D.; Zhao, Y.; Xu, Y. RNA Modification in Metabolism. *MedComm (2020)* **2025**, *6*, e70135.

18. Luo, G.; Hong, T.; Yu, L.; Ren, Z. FTO Regulated Intramuscular Fat by Targeting APMAP Gene via an m(6)A-YTHDF2-dependent Manner in Rex Rabbits. *Cells* **2023**, *12*.

19. Meng, C.; Yang, D. Current Insights into Obesity and m(6)A Modification. *Biomedicines* **2025**, *13*.

20. Ming, X.; Chen, S.; Li, H.; Wang, Y.; Zhou, L.; Lv, Y. m6A RNA Methylation and Implications for Hepatic Lipid Metabolism. *DNA Cell Biol* **2024**, *43*, 271-278.

21. Scheidl, T. B.; Wager, J. L.; Thompson, J. A. Adipose Tissue Stromal Cells: Rheostats for Adipose Tissue Function and Metabolic Disease Risk. *Can J Cardiol* **2025**, *41*, 1727-1735.

22. Sotak, M.; Clark, M.; Suur, B. E.; Borgeson, E. Inflammation and resolution in obesity. *Nat Rev Endocrinol* **2025**, *21*, 45-61.

23. Tan, J.; Shi, C.; Wang, G.; Zhang, L.; Li, F.; Yan, G.; Jin, Y.; Ding, H.; Jiang, F.; Li, X. FTO mediates m6A demethylation of HNF1A and drives hepatic steatosis in metabolic dysfunction-associated steatotic liver disease. *Biochim Biophys Acta Mol Cell Biol Lipids* **2026**, *1871*, 159732.

24. Tao, Y.; Zang, J.; Wang, T.; Song, P.; Zhou, Z.; Li, H.; Wang, Y.; Liu, Y.; Jie, H.; Kuang, M.; Zhao, H.; Wang, F.; Dai, S.; Guo, C.; Zhu, F.; Mao, H.; Liu, F.; Zhang, L.; Wang, Q. Obesity-associated macrophages dictate adipose stem cell ferroptosis and visceral fat dysfunction by propagating mitochondrial fragmentation. *Nat Commun* **2025**, *16*, 7564.

25. Tao, Y.; Zhao, J.; Yin, J.; Zhou, Z.; Li, H.; Zang, J.; Wang, T.; Wang, Y.; Guo, C.; Zhu, F.; Dai, S.; Wang, F.; Zhao, H.; Mao, H.; Liu, F.; Zhang, L.; Wang, Q. Hepatocyte TIPE2 is a fasting-induced Raf-1 inactivator that drives hepatic gluconeogenesis to maintain glucose homeostasis. *Metabolism* **2023**, *148*, 155690.

26. Wang, Y.; Wang, Y.; Gu, J.; Su, T.; Gu, X.; Feng, Y. The role of RNA m6A methylation in lipid metabolism. *Front Endocrinol (Lausanne)* **2022**, *13*, 866116.

27. Xie, D.; Yang, K.; Xu, Y.; Li, Y.; Liu, C.; Dong, Y.; Chi, J.; Yin, X. N6-methyladenosine demethylase fat mass and obesity-associated protein suppresses hyperglycemia-induced endothelial cell injury by inhibiting reactive oxygen species formation via autophagy promotion. *J Diabetes Complications* **2024**, *38*, 108801.

28. Xu, L.; Pan, F.; Guo, Z. TIPE2: A Candidate for Targeting Antitumor Immunotherapy. *J Immunol* **2024**, *212*, 755-763.

29. Xu, S.; Lu, F.; Gao, J.; Yuan, Y. Inflammation-mediated metabolic regulation in adipose tissue. *Obes Rev* **2024**, *25*, e13724.

30. Yang, Q.; Saaoud, F.; Lu, Y.; Pu, Y.; Xu, K.; Shao, Y.; Jiang, X.; Wu, S.; Yang, L.; Tian, Y.; Liu, X.; Gillespie, A.; Luo, J. J.; Shi, X. M.; Zhao, H.; Martinez, L.; Vazquez-Padron, R.; Wang, H.; Yang, X. Innate immunity of vascular smooth muscle cells contributes to two-wave inflammation in atherosclerosis, twin-peak inflammation in aortic aneurysms and trans-differentiation potential into 25 cell types. *Front Immunol* **2023**, *14*, 1348238.

31. Yang, X.; Wang, X.; Tang, H.; Tu, S.; Yin, K.; Zhu, X. m(6)A in adipose tissue inflammation: A novel regulator of obesity and metabolic diseases (Review). *Int J Mol Med* **2026**, *57*.

32. Yang, Z.; Yu, G. L.; Zhu, X.; Peng, T. H.; Lv, Y. C. Critical roles of FTO-mediated mRNA m6A demethylation in regulating adipogenesis and lipid metabolism: Implications in lipid metabolic disorders. *Genes Dis* **2022**, *9*, 51-61.

33. Zeng, Q.; Yang, Y.; Zhang, Y.; Jiang, S. The role of m(6)A in lipid metabolism-related diseases. *SLAS Discov* **2025**, *35*, 100257.

34. Zhou, J.; Chen, P.; Li, Z.; Zuo, Q. Gene delivery of TIPE2 attenuates collagen-induced arthritis by modulating inflammation. *Int Immunopharmacol* **2020**, *79*, 106044.

35. Zhu, S.; Li, W.; Hao, Y.; Zhang, L.; Gao, P. TIPE2 suppresses ferroptosis and pro-inflammatory polarization in macrophages triggered by SARS-CoV-2 spike protein. *Sci Rep* **2025**, *15*, 30246.

36. Zhu, Y.; Wan, F.; Liu, J.; Jia, Z.; Song, T. The Critical Role of Lipid Metabolism in Health and Diseases. *Nutrients* **2024**, *16*.

Supplementary Files

This is a list of supplementary files associated with this preprint. Click to download.

- Table2.docx
- Table1.docx
- Originalblot.pdf
- Supplementarymaterial.docx
- Videoabstract.mp4